

Anti-Ferromagnetic RuO₂: A Stable and Robust OER Catalyst over a Large Range of Surface Terminations

Qihua Liang, Anja Bieberle-Hütter,* and Geert Brocks*



Cite This: *J. Phys. Chem. C* 2022, 126, 1337–1345



Read Online

ACCESS |



Metrics & More

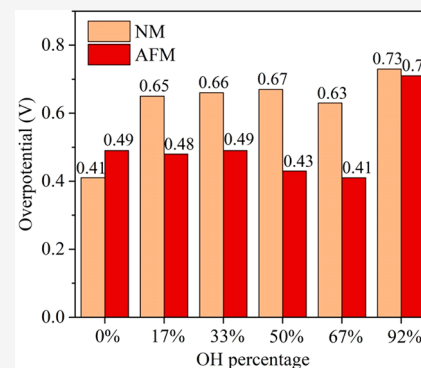


Article Recommendations



Supporting Information

ABSTRACT: Rutile RuO₂ is a prime catalyst for the oxygen evolution reaction (OER) in water splitting. Whereas RuO₂ is typically considered to be non-magnetic (NM), it has recently been established as being anti-ferromagnetic (AFM) at room temperature. The presence of magnetic moments on the Ru atoms signals an electronic configuration that is markedly different from what is commonly assumed, the effect of which on the OER is unknown. We use density functional theory (DFT) calculations within the DFT+U approach to model the OER process on NM and AFM RuO₂(110) surfaces. In addition, we model the thermodynamic stability of possible O versus OH terminations of the RuO₂(110) surface and their effect on the free energies of the OER steps. We find that the AFM RuO₂(110) surface gives a consistently low overpotential in the range 0.4–0.5 V, irrespective of the O versus OH coverage, with the exception of a 100% OH-covered surface, which is, however, unlikely to be present under typical OER conditions. In contrast, the NM RuO₂(110) surface gives a significantly higher overpotential of ~0.7 V for mixed O/OH terminations. We conclude that the magnetic moment of RuO₂ supplies an important contribution to obtaining a low overpotential and to its insensitivity to the exact O versus OH coverage of the (110) surface.



INTRODUCTION

Efficient catalysis of the oxygen evolution reaction (OER) is important in the electrochemical production of fuels for storage of renewable energy. The OER, which constitutes a critical step in such electrochemical processes, has been the subject of many theoretical and experimental studies aimed at developing electrocatalysts with improved activity.^{1–3} Ruthenium dioxide (RuO₂) has been widely reported to be one of the best anode materials for catalyzing the OER in water splitting, having an excellent electrocatalytic activity in both acidic and basic media.^{2,4–7} Despite the relatively high cost of ruthenium obstructing large-scale commercial applications, RuO₂ continues to be an important material, against which future (cheaper) OER catalysts need to be benchmarked.

RuO₂ has long been considered to be a paramagnetic metal,^{8,9} and most theoretical investigations assume a non-magnetic (NM) ground state for RuO₂ when investigating its OER performance on the atomic scale.^{5,10–13} A recent experimental neutron diffraction study on RuO₂ single crystals, combined with density functional theory (DFT) calculations, has established that RuO₂ is an anti-ferromagnet (AFM) at room temperature.¹⁴ Magnetism and magnetic ordering are not likely to influence the energetics of the OER directly, but the presence of substantial magnetic moments signals a preference for a local high-spin electronic configuration on the Ru atoms. The latter has a distribution of electrons over the energy levels that is different from that of the low-spin configuration assumed in calculations with a NM ground state.

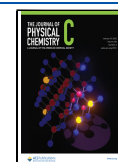
This difference in electron configurations on the Ru atoms can affect the OER energetics. Indeed, a DFT study on the final step in the OER, the formation of an O₂ molecule from an adsorbed OOH species, has concluded that the formation energy on a ferromagnetic (FM) RuO₂(110) surface is ~1 eV lower than that on its NM counterpart.¹⁵ This strongly suggests that it is important to include the true magnetic electronic ground state to elucidate the success of RuO₂ as a catalyst for the OER.

RuO₂ has a rutile structure, and its most prominent surface for the OER is the (110) surface.^{5,12,15} The unit cell of the stoichiometric (110) surface contains two differently coordinated Ru atoms, one that is 6-fold coordinated by O atoms and one with a 5-fold coordination. The latter, coordinatively unsaturated (CUS), surface Ru atom is exposed and thought to be a reaction center for the OER.¹⁶ This clean surface, with exposed Ru atoms, does not persist under electrochemical conditions, as it will be covered by O or OH species, or a mixture of the two.^{5,13,17–19} Early DFT calculations of the OER on NM RuO₂ showed a difference of only ~0.1 V in the

Received: October 4, 2021

Revised: January 7, 2022

Published: January 16, 2022



overpotential between a fully O-terminated surface and a fully OH-terminated surface.¹² Later, more refined, calculations on NM RuO₂ identified a more advantageous reaction path, where an adsorbed OOH species transfers its H atom to a neighboring O site on the surface.⁵ Obviously, such an event can only take place if a neighboring O site is available, as OH sites block this transfer. This makes it necessary to revisit the phase diagram of O vs OH termination of the RuO₂(110) surface, and its effect on the OER process.

In the present paper, we study the OER on the AFM RuO₂(110) surface by means of DFT calculations. We establish the electronic structure and the magnetic moments of the surface Ru atoms as a function of O/OH coverage and calculate the O/OH coverage as a function of the applied potential and the pH (Pourbaix diagram). We investigate the entire OER, calculate the free energies of all reaction steps involved, and determine the overpotential, which is the prime parameter to judge the electrochemical activity toward the OER.²⁰ In addition, we explore the dependence of the free energies and overpotential on the OH surface coverage and surface phases of the RuO₂(110) surface. We show that the AFM RuO₂(110) surface is more active for the OER than a NM RuO₂(110) surface. Except for the fully OH-terminated surface, the surface configuration has in fact little effect in determining the electrocatalytic activity of AFM RuO₂ toward the OER, explaining the versatility of this material under different pH conditions.

COMPUTATIONAL DETAILS

The DFT calculations are carried out with the Vienna Ab Initio Simulation Package (VASP), which uses the projector-augmented plane wave (PAW) technique, and a plane wave basis set.^{21–23} DFT exchange and correlation are treated at the level of the generalized gradient approximation (GGA), using the Perdew–Burke–Ernzerhof (PBE) functional.²⁴ Following ref 14, to better model on-site electron–electron repulsion, which is instrumental in correctly describing the magnetism in RuO₂, we use the DFT+*U* approach in the form proposed by Dudarev et al.,²⁵ with an on-site interaction parameter of $U - J = 2.0$ eV for Ru. As shown in ref 14, the total energy difference between NM and AFM-ordered RuO₂ increases with increasing value of $U - J$, but for too large a value, RuO₂ becomes a semiconductor, rather than a metal. The value $U - J = 2.0$ eV has been selected such that the NM–AFM total energy difference is a few times $k_B T$ (at room temperature) per formula unit, and RuO₂ is still metallic. As PAW potentials, we use the Ru_{pv} potential, which includes p semicore states, and standard potentials for O and H atoms. We employ a plane-wave kinetic energy cutoff of 500 eV and energy and force convergence criteria of 10⁻⁵ eV and 0.01 eV/Å, respectively. The optimized RuO₂ bulk lattice parameters are $a = 4.53$ Å and $c = 3.12$ Å, in good agreement with the experimental values, $a = 4.49$ Å and $c = 3.11$ Å.²⁶

To model the (110) surface, a seven-layer stoichiometric RuO₂ slab is constructed with (110) surfaces, a 3 × 2 rectangular surface supercell (cell parameters 9.36 and 12.82 Å), and a 15 Å vacuum region. A 4 × 3 × 1 Monkhorst–Pack sampling of the reciprocal cell is used.²⁷ The atomic positions of the four bottom layers of the RuO₂ slab are fixed, and all other atomic positions are relaxed to their minimum energy positions. The rutile structure allows for only one particular AFM ordering in bulk RuO₂ that does not enlarge the size of the (bulk crystal) unit cell with respect to the NM unit cell; see

Figure S1. As this is the AFM ordering determined from spin-polarized neutron diffraction,¹⁴ we adopt it for our calculations. We transfer the spin arrangement found for bulk RuO₂ to the seven-layer RuO₂(110) slab, as indicated by down (orange) and up (blue) arrows at the Ru sites shown in Figure 1. The

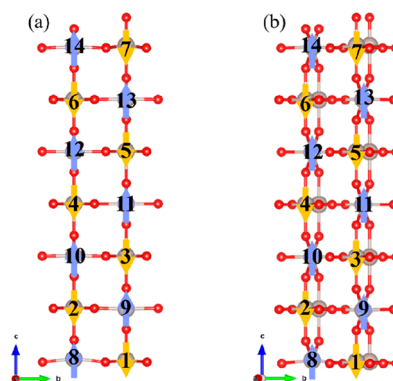


Figure 1. (a) Front and (b) rotated views of the unit cell of a seven-layer RuO₂(110) slab; the (fully oxygen-covered) OER active surface is at the top. The gray and red spheres represent Ru and oxygen atoms, respectively. AFM spin arrangements are indicated by down (orange) and up (blue) arrows at the Ru sites. The numbers represent the Ru atoms in Table 1.

size of the magnetic moments on the Ru atoms changes during the (electronic) optimization, but this AFM ordering persists. Convergence tests regarding the size of the slab and supercell are presented in the Supporting Information. Tables S1–S3 give the calculated magnetic moments on the Ru atoms of bulk RuO₂ and of RuO₂ slabs of varying thickness, and Figures S1–S3 show the corresponding atomic structures.

RESULTS AND DISCUSSION

RuO₂(110) Surface. Magnetism. Starting with bulk RuO₂, we find that the AFM state is 74 meV per formula unit lower in energy than the (non-spin-polarized) NM state, with magnetic moments on the Ru atoms of $\pm 1.18 \mu_B$, which is in agreement with previous work.¹⁴ Proceeding with the surface, the slab used to model the (110) surface is shown in Figure 1. It has a fully O-terminated surface on one side, which is a stable surface termination under high pH and overpotential conditions; see below. This surface contains two structurally different Ru atoms, indicated by the labels 7 and 14 in Figure 1. We maintain the stoichiometry of RuO₂ in the slab, so the surface on the other side (Ru atoms 1 and 8) remains clean of O atoms.

The optimized magnetic moments of the Ru atoms in the slab are shown in Table 1. The AFM ordering persists throughout the slab, with the magnetic moments in the middle of the slab (Ru atoms 4 and 11) attaining values of around $\pm 1.18 \mu_B$, which is similar to the bulk. Toward the surfaces of the slab, the absolute magnetic moments become somewhat

Table 1. Magnetic Ordering and Moments on the Ru Atoms in the RuO₂(110) Slab (See Figure 1)^a

Ru atoms	magnetic moment (μ_B)
1–7	−0.91, −0.91, −1.15, −1.17, −1.11, −1.12, −0.22
8–14	1.18, 1.09, 1.18, 1.18, 1.16, 1.16, 1.45

^aPositive/negative signs stand for spin-up/down.

smaller but stay close to their bulk value. The exceptions are the Ru atoms 14 and 7 at the O-terminated surface, which have magnetic moments of $1.45 \mu_B$ and $-0.22 \mu_B$, respectively, signifying that their absolute values are $0.27 \mu_B$ larger, respectively, $0.95 \mu_B$ smaller than the bulk value. Especially the latter large change likely indicates a significant change in the electronic structure of the surface atom.

A Ru ion in bulk RuO_2 has a nominal oxidation state of 4+, corresponding to a configuration of $5s^0 4d^4$.²⁸ The partial density of states (PDOS) of Ru atom 4, which is in the middle of the slab and thus bulk-like, is shown in Figure 2a. In the

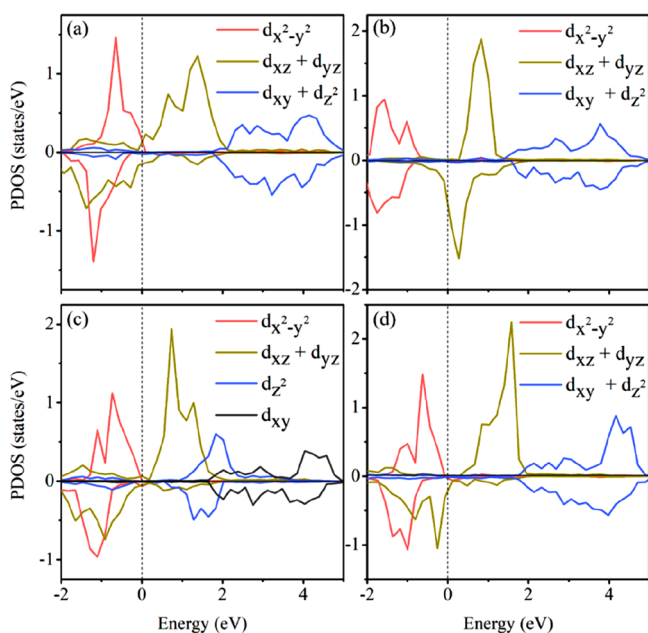


Figure 2. (a) Spin-polarized projected density of states (PDOS) of a Ru atom in the middle of the slab (Ru atom 4 in Figure 1). PDOS of the OER-active surface Ru atom (Ru atom 7 in Figure 1) (b) with an adsorbed O atom on top, (c) with an O vacancy, and (d) with an adsorbed OH species on top.

rutile structure, a Ru atom is 6-fold coordinated by oxygen atoms in a distorted octahedral coordination with O–Ru–O angles of 78 and 102°. Perfect octahedral coordination gives a $t_{2g}-e_g$ splitting of the d-states, and the distortion splits the multiplet further, so that the energy ordering of the d-states on Ru atom 4 (referring to the axes used in Figure 1) is $d_{x^2-y^2} < d_{xz}, d_{yz} < d_{xy}, d_{z^2}$, which corresponds to what is found in bulk RuO_2 .¹⁴ As can be observed in Figure 2a, for Ru atom 4, the $d_{x^2-y^2}$ spin-up and spin-down orbitals are fully occupied, whereas only the spin-down d_{xz} and d_{yz} orbitals are occupied, which indeed corresponds to a d^4 configuration. Note however that, instead of a magnetic moment of $-2 \mu_B$, which one expects to find for a purely ionic $\text{Ru}^{4+}(\text{O}^{2-})_2$, we find $-1.17 \mu_B$, reflecting the significant hybridization of the Ru d-orbitals with their surroundings.

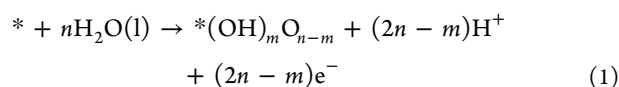
This basic electronic structure holds for all Ru atoms in the system, with the exception of the surface Ru atom 7. Its PDOS, shown in Figure 2b, indicates a full occupancy of $d_{x^2-y^2}$ spin-up and spin-down but only a partial occupancy of spin-down d_{xz} and d_{yz} , consistent with a configuration $d \lesssim 3$ and oxidation state $\gtrsim 5+$. This increased oxidation state explains the small magnetic moment of $-0.22 \mu_B$ observed on Ru atom 7. The O atom on top is bonded only to this particular Ru atom, see

Figure 1, which likely causes its increased oxidation. All other O atoms in the structure are bonded to two neighboring Ru atoms.

Ru atom 7 represents an active site for the OER, implying that over the course of the OER (to be discussed in detail below) the O atom adsorbed on top is replaced by an OH or OOH species, or becomes a vacancy, thereby creating a coordinatively unsaturated (CUS) surface Ru atom. Interestingly, replacing the O atom by OH or OOH or creating a vacancy restores the basic electronic configuration of the Ru atom. The calculated magnetic moments of CUS Ru and Ru with OH adsorbed on top are $-1.21 \mu_B$ and $-1.26 \mu_B$, respectively, close to the bulk value. The corresponding PDOSs, Figure 2c,d, are consistent with valency 4+, and are in fact very similar to that of a Ru atom in the middle of the slab, Figure 2a. In conclusion, from the PDOS and magnetic moments analysis, we find that the electronic configuration of the CUS Ru atom is affected by O adsorption but not much by OH adsorption.

Surface Termination. Though the $\text{RuO}_2(110)$ surface is mostly thought of as O-terminated under OER conditions,^{5,10,15} experiments also find a mixed O/OH surface termination under certain conditions.^{5,17,18} The exact coverage by O or OH depends upon the applied potential, as is concluded from in situ surface X-ray scattering experiments combined with DFT calculations.⁵ Previous calculations have used a NM RuO_2 substrate and considered a small number of fixed O/OH terminations.¹³ Here, we focus on AFM RuO_2 , consider a wide range of O/OH terminations, and incorporate the entropies of the O/OH coverages to calculate their free energies.

The relative stability of different terminations can be inferred from studying the adsorption of n water molecules on the N sites of an O/OH-free surface in the form of m OH groups and $n - m$ O groups, as in the reaction



where $*$ indicates the O/OH-free surface and $*(\text{OH})_m\text{O}_{n-m}$ the surface with mixed O/OH coverage. Applying the computational hydrogen electrode (CHE) approach, one refers the potential of the RuO_2 electrode with respect to the reversible hydrogen electrode (RHE), which sustains the equilibrium $\text{H}^+ + \text{e}^- \leftrightarrow \frac{1}{2}\text{H}_2$ under standard conditions ($T = 298 \text{ K}$, $p_{\text{H}_2} = 1 \text{ bar}$).²⁹ In addition, an equilibrium between liquid and gaseous water is assumed, $\text{H}_2\text{O}(\text{l}) \leftrightarrow \text{H}_2\text{O}(\text{g})$ ($T = 298 \text{ K}$, $p_{\text{H}_2\text{O}} = 0.035 \text{ bar}$).

The Gibbs free energy of reaction 1 can then be expressed as

$$G(n, m) = E(*(\text{OH})_m\text{O}_{n-m}) + \text{ZPE} - \text{TS}(n, m) + (2n - m) \left[\frac{1}{2} \mu_{\text{H}_2(\text{g})} - eU_{\text{RHE}} \right] - E(*) - n\mu_{\text{H}_2\text{O}(\text{g})} \quad (2)$$

where $E(*(\text{OH})_m\text{O}_{n-m})$ and $E(*)$ are the DFT total energies of the O/OH-covered $\text{RuO}_2(110)$ and the O/OH-free surface, respectively. $\text{ZPE} = \text{ZPE}_{\text{right}} - \text{ZPE}_{\text{left}}$ is the zero-point energy correction, with $\text{ZPE}_{\text{left/right}}$ being the zero-point vibrational energies of all species on the left and right sides of reaction 1, respectively. These vibrational energies can be expressed as

$\sum_i \frac{1}{2} h\nu_i$, with ν_i being the vibrational frequency and h Planck's constant. In principle, the sum runs over all vibrational modes of the system, but in practice, only the modes involving hydrogen have a frequency sufficiently high to give an appreciable contribution. In our case, the only hydrogen-containing species are the adsorbed species and the free water and hydrogen molecules, for which we then calculate the vibrational modes and the ZPE. Furthermore, $\mu_{\text{H}_2(\text{g})}$ and $\mu_{\text{H}_2\text{O}(\text{g})}$ are the chemical potentials of hydrogen gas and water gas, obtained from the DFT total energies and ZPEs of the molecules and the tabulated properties of the gases; U_{RHE} is the potential of the RuO_2 electrode with respect to the RHE.²⁹ The entropy $S(n, m)$ is modeled as the sum of the vibrational entropy^{30,31} and the mixing entropy.

We find that mixed O/OH coverages are energetically favorable only on a fully covered surface ($n = N$) and the O/OH configurations at fixed OH concentration (fixed m) differ little in energy ($\lesssim 0.1$ eV), so we use the simple expression

$$S_{\text{mix}}(N, m) = -Nk_{\text{B}} \left[\frac{m}{N} \ln \left(\frac{m}{N} \right) + \frac{N-m}{N} \ln \left(\frac{N-m}{N} \right) \right] \quad (3)$$

Creating uncovered Ru sites on the surface ($n < N$) is energetically favorable only in the case of a fully OH-covered surface ($n = m$), and then far more favorable CUS Ru atoms (Ru atom 7 in Figure 1). So, for that particular case, we use the mixing entropy

$$S'_{\text{mix}}(n, n) = -\frac{1}{2} Nk_{\text{B}} \left[\frac{2n-N}{N} \ln \left(\frac{2n-N}{N} \right) + \frac{2N-2n}{N} \ln \left(\frac{2N-2n}{N} \right) \right]; \quad n = \frac{N}{2}, \dots, N \quad (4)$$

where the factors 2 originate from the fact that only half of the Ru sites on the (110) surface are CUS Ru atoms.

The pH dependence of the free energy, eq 2, can be made explicit by referring the RHE to the standard hydrogen electrode (SHE) (pH 0) by the standard expression

$$\begin{aligned} -eU_{\text{RHE}} &= -eU_{\text{SHE}} + k_{\text{B}}T \ln a_{\text{H}^+} \\ &= -eU_{\text{SHE}} - (\text{pH}) \times k_{\text{B}}T \ln 10 \end{aligned} \quad (5)$$

The values m, n that give the minimum $G(n, m)$ represent the most stable surface O/OH coverage.

Starting from the fully O-covered surface, we have studied mixed O/OH/vacancy coverages; a number of representative structures are shown in Figure 3. A Pourbaix diagram of the most stable coverages, as a function of U_{SHE} and pH, is shown in Figure 4. A fully O coverage is most stable above $U_{\text{SHE}} \approx 1.3$ V at pH 0, dropping linearly to above $U_{\text{SHE}} \approx 0.5$ V at pH 14. Between $U_{\text{SHE}} \approx 0.4$ and 1.1 V, a full OH coverage is most stable at pH 0, and that interval drops linearly to between $U_{\text{SHE}} \approx -0.4$ and 0.3 V at pH 14. In the intermediate voltage ranges ($1.1 \text{ V} \lesssim U_{\text{SHE}} \lesssim 1.3 \text{ V}$ at pH 0 to $0.3 \text{ V} \lesssim U_{\text{SHE}} \lesssim 0.5 \text{ V}$ at pH 14), mixed O/OH coverages are stable. Below the line $U_{\text{SHE}} \approx 0.4$ V at pH 0 to $U_{\text{SHE}} \approx -0.4$ V at pH 14, it becomes increasingly advantageous to create uncovered Ru sites, but a surface configuration where all CUS Ru atoms are uncovered only becomes stable below the line $U_{\text{SHE}} \approx -0.5$ V at pH 0 to $U_{\text{SHE}} \approx -1.1$ V at pH 14.

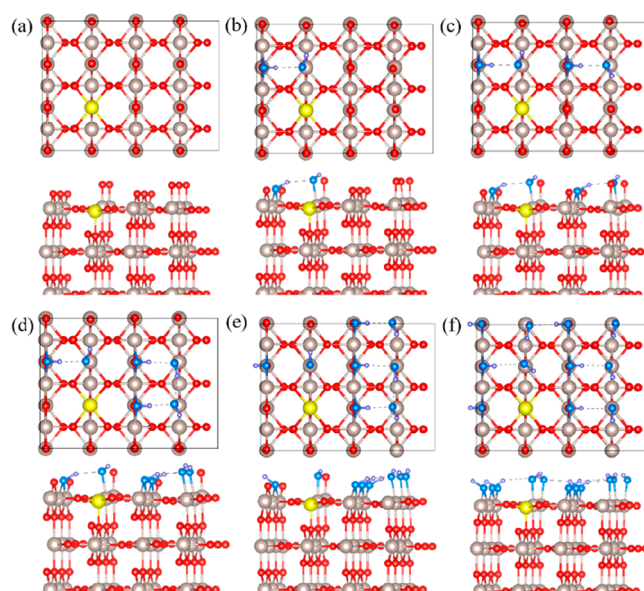


Figure 3. Top and side views of (110) surfaces with different O/OH terminations in a 3×2 supercell: (a) 100/0%, (b) 83/17%, (c) 67/33%, (d) 50/50%, (e) 33/67% (f) 8/92% O/OH termination. The OH groups are marked by blue O and purple H atoms, with dashed lines indicating hydrogen bonds. An active Ru site is singled out and highlighted in yellow.

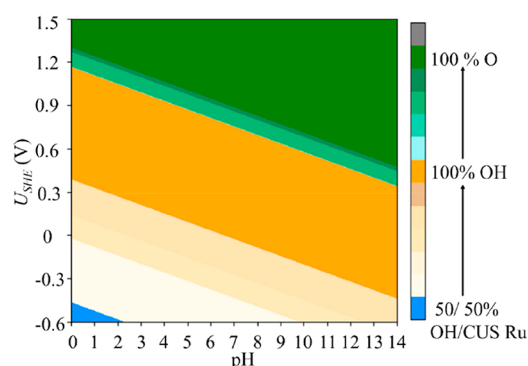


Figure 4. Pourbaix diagram depicting the most stable $\text{RuO}_2(110)$ surface covering as a function of pH and potential U_{SHE} (V). The dark green, orange, and blue colors indicate regions where, respectively, 100% O-covered, 100% OH-covered, and 50/50% CUS/OH-covered Ru sites are thermodynamically most stable. The lighter green colors indicate a transition region where, starting from 100% OH coverage, the % OH gradually decreases and the % O increases. The lighter orange colors indicate a similar transition region between the 50/50% free/OH-covered and 100% OH-covered surfaces, where the % of free Ru sites gradually decreases.

In experiments, the OER on RuO_2 is typically measured in the interval $U_{\text{RHE}} = 0.2\text{--}1.6$ V, which translates into the same interval for U_{SHE} at pH 0 to 0.6–0.8 V at pH 14; see eq 5. The lowest part of this interval corresponds to a OH-covered surface with a small number of uncovered CUS Ru atoms; see Figure 4. In the range $U_{\text{RHE}} = 0.4\text{--}1.1$ V, one has a fully OH-covered surface, from 1.1 to 1.3 V one has mixed O/OH coverage with an increasing O percentage, and above 1.3 V the fully O-covered surface is most stable. These results actually agree quite well with what has been found in an experimental study.⁵

OER Reaction. We consider a four-electron reaction mechanism for OER under alkaline conditions.^{32–34} The

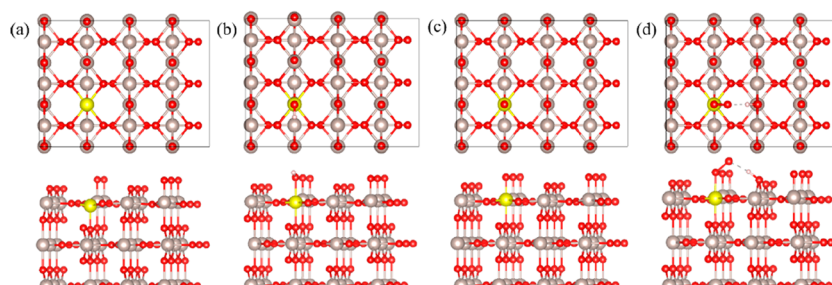
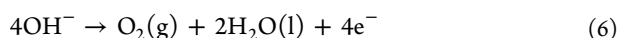
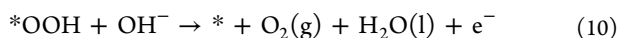
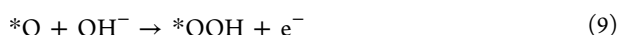
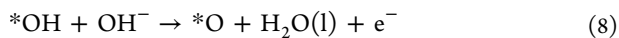


Figure 5. Top and side views of the OER reaction cycle, eqs 7–10, for a O-covered surface, (a) the active CUS (uncovered) Ru atom highlighted in yellow, (b) with OH, (c) O, and (d) OOH adsorbed. The dashed line between O and H in part d indicates the transfer of H to a neighboring O site.

outcomes are easily adapted to the reaction mechanism under acidic conditions.³² The overall water oxidation reaction is



where (g) and (l) refer to the gas and liquid phases, respectively. The reaction proceeds in four steps³²



where * represents the active site of the catalyst, in this case a CUS Ru site on the surface, and *OH, *O, and *OOH represent the species adsorbed on the active site. As in the previous section, we use the CHE approach, assuming the equilibrium $\text{H}^+ + \text{e}^- \leftrightarrow \frac{1}{2}\text{H}_2$ under standard conditions ($T = 298 \text{ K}$, $p_{\text{H}_2} = 1 \text{ bar}$),²⁹ as well as equilibrium between liquid and gaseous water, $\text{H}_2\text{O}(\text{l}) \leftrightarrow \text{H}_2\text{O}(\text{g})$ ($T = 298 \text{ K}$, $p_{\text{H}_2\text{O}} = 0.035 \text{ bar}$). Referring the potential of the RuO_2 electrode with respect to the reversible hydrogen electrode (RHE), the Gibbs free energies, ΔG_n , of reactions 6–10 are given by

$$\Delta G_1 = E_{*\text{OH}} - E_* - E_{\text{H}_2\text{O}} + \frac{1}{2}E_{\text{H}_2} + (\Delta\text{ZPE} - T\Delta\text{S})_1 - eU_{\text{RHE}} \quad (11)$$

$$\Delta G_2 = E_{*\text{O}} - E_{*\text{OH}} + \frac{1}{2}E_{\text{H}_2} + (\Delta\text{ZPE} - T\Delta\text{S})_2 - eU_{\text{RHE}} \quad (12)$$

$$\Delta G_3 = E_{*\text{OOH}} - E_{*\text{O}} - E_{\text{H}_2\text{O}} + \frac{1}{2}E_{\text{H}_2} + (\Delta\text{ZPE} - T\Delta\text{S})_3 - eU_{\text{RHE}} \quad (13)$$

$$\Delta G_4 = \Delta G_0 - \Delta G_1 - \Delta G_2 - \Delta G_3 - 4eU_{\text{RHE}} \quad (14)$$

where $\Delta G_0 = 4.92 \text{ eV}$ is the Gibbs free energy of the overall reaction 1; E_* , $E_{*\text{OH}}$, $E_{*\text{O}}$, and $E_{*\text{OOH}}$ are the total energies of the surface and of surfaces with the single adsorbed species OH, O, and OOH, respectively, and $E_{\text{H}_2\text{O}}$ and E_{H_2} are the total energies of the H_2O and H_2 molecules, all obtained from DFT calculations. Note that we use eq 14 to avoid having to calculate the total energy of the O_2 molecule, whose triplet ground state is described less accurately in the current approach. ΔZPE and $T\Delta\text{S}$ are the changes in zero-point energies and entropy from the initial state to the final state,

respectively, with T being the temperature. In addition, ΔS contains the entropy contributions of the gas phases used in reactions 7–10.^{30,31}

For an ideal catalyst, the four reaction steps have an equally large ΔG_n

$$\frac{G_0}{4} = \Delta G_1 = \Delta G_2 = \Delta G_3 = \Delta G_4 = 1.23 \text{ eV} \quad (15)$$

such that a single potential $U_0 = 1.23 \text{ V}$ drives all reaction steps. Normally, this is not the case, and an additional overpotential is required to drive the step with the largest ΔG_n . The overpotential is then defined by

$$\eta = \frac{1}{e} \max_{n=1,2,3,4} [\Delta G_n] - U_0 \quad (16)$$

Free Energies and Overpotentials. We start from the fully O-covered $\text{RuO}_2(110)$ surface with one active Ru site, which either is uncovered or adsorbs one of the intermediate species, *OH, *O, and *OOH, according to reactions 7–10, as shown in Figure 5. Upon geometry optimization, the H atom of an adsorbed OOH species transfers spontaneously to an adjacent O–Ru site on the surface, leaving behind an OO species adsorbed on the active site (see Figure 5d), which agrees with the results obtained by Rao et al.⁵ In fact, such a spontaneous H transfer leaving behind an OO species also happens on mixed O/OH terminated surfaces, as long as there is an O-terminated Ru site neighboring the active Ru site. Only if such an O-terminated Ru site is not available, as on a fully OH-terminated surface, the OOH adsorbs without splitting off the H; see Figure S4.

Figure 6 shows the Gibbs free energies of reactions 11–14, calculated at zero potential ($U_{\text{RHE}} = 0$), and the calculated overpotential, eq 16, for mixed O/OH-covered $\text{RuO}_2(110)$ surfaces, with 0–100% fractions OH coverage, and an AFM $\text{RuO}_2(110)$ substrate. In order to analyze the effects of magnetism on the $\text{RuO}_2(110)$ surface for the OER, we have repeated the calculations switching off the spin polarization, which makes the RuO_2 substrate NM. The fully O-terminated (0% OH) NM surface has an overpotential of 0.41 V, which agrees with literature results,^{5,12} where the potential determining step (PDS) is the final reaction step, eq 10, Figure 6a. Partially OH-covered surfaces display higher overpotentials between 0.63 and 0.73 V, where the third reaction step, eq 9, is the PDS. These higher overpotentials disagree with the experimental observations regarding the OER activity of RuO_2 . However, they agree with the fact that DFT calculations on NM RuO_2 consistently predict larger overpotentials, as discussed in ref 35.

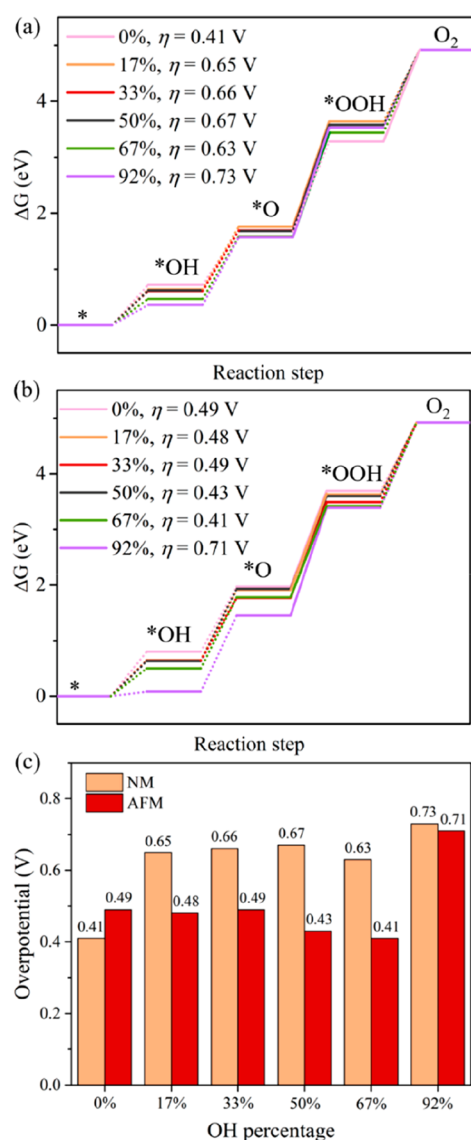


Figure 6. Gibbs free energies of the four reaction steps, eqs 11–14, of (a) NM and (b) AFM systems with mixed O/OH coverages and different OH percentages. The values of the overpotential are given in the legends. The potential determining steps are represented by the solid lines between the steps. (c) Summary plot of the overpotentials of the NM and AFM systems.

For the AFM configuration, the fully O-terminated (0% OH) surface has an overpotential of 0.49 V, which is close to the NM configuration but different from the latter; the PDS is the third reaction step, eq 9, Figure 6b. In addition, the overpotential calculated for AFM RuO₂ decreases slightly to 0.41 V, for increasingly OH-covered surfaces, the third reaction step remaining the PDS. These low overpotentials of different surface terminations agree well with the experimental results that RuO₂ is an OER active material. The cause of the difference in overpotential between the calculations of AFM and NM RuO₂ is analyzed in the next section. Only close to a fully covered ($\geq 92\%$) OH surface does the overpotential increase to 0.71 V. This higher overpotential stems from the fact that, if OOH adsorbs on the top of the Ru active site, the proton of the OOH group transfers to an O on an adjacent Ru site, Figure 5d, as discussed above. This route is blocked for a

fully covered OH surface and forces OOH to adsorb as one species, which increases its energy.

Introducing magnetism in RuO₂ does not affect the OER on a fully O-covered (110) surface much, but it considerably reduces the overpotential on mixed O/OH-covered surfaces, Figure 6c. A fully O-covered surface is maximally oxidized, resulting in very small magnetic moments on the CUS Ru atoms (Ru atom 7 in Figure 1), where the difference in the electronic configuration between AFM and NM states is small, Figure 2b. As discussed in the Magnetism section, on mixed O/OH-covered surfaces, the average oxidation state of the CUS Ru atoms decreases, and the increased number of electrons prefer to be in a high-spin state, as is signaled by the magnetic moments on the CUS Ru atoms, Figure 2d. Whereas this is correctly taken into account in the AFM calculation, in a NM calculation, one enforces a low-spin configuration on these atoms, which introduces an error, as this is not the true ground state. The results discussed here are obtained with a 3×2 surface supercell. Using a smaller 2×1 supercell, as in ref 5, for instance, the results are qualitatively similar but quantitatively a little different, as discussed in the Supporting Information; see Figures S5 and S6. Using a larger supercell increases the accuracy of the calculations.

Adsorption Energies. In order to interpret the trends in the calculated overpotentials, it is instructive to examine the adsorption free energies of the OER intermediates.³⁶ These can be easily extracted from the Gibbs free energies of the reaction steps, eqs 11–14, setting $U_{RHE} = 0$

$$\begin{aligned} \Delta G_{*OH} &= \Delta G_1 \\ &= E_{*OH} - E_* - E_{H_2O} + \frac{1}{2}E_{H_2} \\ &\quad + (\Delta ZPE - T\Delta S)_1 \end{aligned} \quad (17)$$

$$\begin{aligned} \Delta G_{*O} &= \Delta G_1 + \Delta G_2 \\ &= E_{*O} - E_* - E_{H_2O} + E_{H_2} + (\Delta ZPE - T\Delta S)_{1+2} \end{aligned} \quad (18)$$

$$\begin{aligned} \Delta G_{*OOH} &= \Delta G_1 + \Delta G_2 + \Delta G_3 \\ &= E_{*OOH} - E_* - 2E_{H_2O} + \frac{3}{2}E_{H_2} \\ &\quad + (\Delta ZPE - T\Delta S)_{1+2+3} \end{aligned} \quad (19)$$

The free energies of the OER intermediates for adsorption on pure and mixed O/OH-covered surfaces are shown in Figure 7. The lower the adsorption free energy, the stronger the bonding of the species to the active site.

Starting with the OH adsorbate, we notice that ΔG_{*OH} decreases with increasing OH coverage from 0.80 eV for a fully O-covered surface (0% OH) to nearly zero for the 92% OH-covered surface; see the bottom panel in Figure 7. This is consistent with the calculated stability of the fully OH-covered surface under zero-potential conditions; see Figure 4. For the ideal catalyst, the ΔG_{*OH} should be close to the ideal value $\Delta G_0/4 = 1.23$ eV, eqs 15 and 17. However, all of the O/OH coverages give a ΔG_{*OH} that is significantly smaller than the ideal value, which means the OH binds to the surface too strongly. Because of the sum rule $\Delta G_{*OH} + \Delta G_2 + \Delta G_3 + \Delta G_4 = \Delta G_0$, eqs 14 and 17, if ΔG_{*OH} is too small, then one or more of the remaining steps, ΔG_i ($i = 2, 3, 4$), have to be too large.

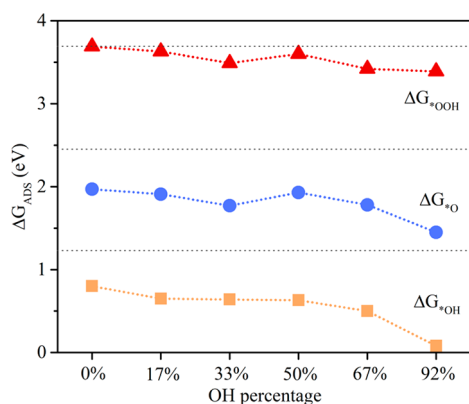


Figure 7. Gibbs free energies of adsorption, ΔG_{ADS}^* , where ADS = OH, O, or OOH. The horizontal black dashed lines stand for the Gibbs free energies 1.23, 2.46, and 3.69 eV, respectively.

Defining the deviation from ideal as $\delta_1 = \left(\frac{\Delta G_0}{4} - \Delta G_{*_{OH}}^*\right)/e$, the overpotential η , eq 16, must be at least $\delta_1/3$ V, as the best scenario is to divide this deviation because of the OH overbinding equally over the three remaining reaction steps.

The next reaction step, following OH adsorption, involves an adsorbed O species. The middle panel in Figure 7 displays the adsorption free energy, $\Delta G_{*_{O}}^*$, of the O species, eq 18. $\Delta G_{*_{O}}^*$ decreases from 1.97 to 1.45 eV upon increasing the surface OH coverage from 0 to 92%, showing a similar trend in the increase of the O binding strength as for the OH species. Comparing to the ideal value $\Delta G_0/2 = 2.46$ eV, eqs 15 and 18, also the O atom is bonded too strongly. Defining a deviation from ideal by $\delta_2 = \left(\frac{\Delta G_0}{2} - \Delta G_{*_{O}}^*\right)/e$, we note that $\delta_2 \approx \delta_1$, so the second reaction step has not compensated for the deviation of the first step at all. On the contrary, following a reasoning similar to that in the previous paragraph, then because of the O overbinding, the overpotential must now be at least $\delta_2/2$ V, if the deviation is divided equally over the two remaining reaction steps.

Finally, the top panel in Figure 7 shows the adsorption free energy, $\Delta G_{*_{OOH}}^*$, of the OOH species, eq 19. The calculated values for $\Delta G_{*_{OOH}}^*$ decrease from 3.69 to 3.39 eV upon increasing the surface OH coverage from 0 to 92%. These values are in fact close to the ideal value $3\Delta G_0/4 = 3.69$ eV, eqs 15 and 19, which means that the systems bind OOH almost perfectly. We define as before the deviation from the ideal value as $\delta_3 = \left(\frac{3\Delta G_0}{4} - \Delta G_{*_{OOH}}^*\right)/e$, where we note that numerically $\delta_3 < \frac{1}{2}\delta_2$. From eqs 18 and 19, we now obtain $\Delta G_3 = \frac{\Delta G_0}{4} + e(\delta_2 - \delta_3)$ and $\Delta G_4 = \frac{\Delta G_0}{4} + e\delta_3$. We conclude that $\Delta G_3 > \Delta G_4$, so the third reaction step, eq 9, determines the overpotential, which is $\eta = \delta_2 - \delta_3$. Notably, this number is fairly constant as a function of OH coverage; see Figure 6b and c. In summary, the overpotential is determined by the fact that the intermediate species O and OH bind to the substrate too strongly.

Repeating this analysis for the OER on NM RuO₂ shows that $\Delta G_{*_{O}}^*$ for AFM RuO₂ is consistently higher than that for NM RuO₂ by up to ~ 0.3 eV for all O/OH coverages, except for the 92% OH coverage; see Figure S7. In contrast, the difference in $\Delta G_{*_{OOH}}^*$ between AFM and NM RuO₂ alternates in sign as a function of increasing OH coverage, whereas Δ

$G_{*_{OH}}^*$ is relatively unaffected. This suggests that the main effect of magnetism is to decrease the bonding strength of the O adsorption, which decreases δ_2 and therefore reduces the overpotential, as caused by the third reaction step, to bring it in agreement with experiment. This finding is consistent with ref 35, where an overbinding of the O adsorbate in DFT calculations on NM RuO₂ has been suggested as a possible cause for the discrepancy in overpotential between these calculations and experiment.

We propose that the differences between the OER results on AFM and NM RuO₂ can be understood from the changes in the electronic structure that accompany the magnetism, Figure 2. As discussed above, switching on spin polarization creates a high-spin state (and magnetic moments) on the OER-active Ru atoms without adsorbate, or with OH/OOH adsorbates; see Figure 2c and d. This lowers the total energies $E_{*_{OH}}$, $E_{*_{O}}$, and $E_{*_{OOH}}$ with respect to their low-spin NM counterparts. The Ru atom with O adsorbate is low spin anyway (see Figure 2b), so the effect on the total energy $E_{*_{O}}$ of switching on spin polarization is minimal. In view of eqs 17–19, the largest effect of switching on spin polarization then should be an increase of $\Delta G_{*_{O}}^*$.

Previous computational studies on metal oxides have found that the O versus OH termination of a surface can strongly modify the overpotential of the OER.^{37–40} For example, Calle-Vallejo et al.³⁹ have studied this for the NiO(001) surface and its hydroxylated modification NiOOH. Pristine NiO shows an overpotential of 0.3 V, while the overpotential increases to 0.6 V for the hydroxylated (NiOOH) surface, demonstrating that hydroxylation of the surface significantly decreases its OER activity. Sun et al.⁴⁰ have investigated the OER on clean, O- and OH-terminated spinel Co₃O₄(100) surfaces. The O-terminated surface gives an overpotential of 0.45 V, whereas OH-terminated and clean surfaces yield much higher overpotentials of 0.93 and 1.82 V, respectively.

Our calculations show that the overpotential obtained for the OER on the RuO₂(110) surface is remarkably insensitive to the exact mix of O versus OH coverage. This can be traced to the fact that the adsorption energies of the intermediate species, OH, O, and OOH, do not change very much upon varying the O/OH coverage mix. The exception to this rule is a fully OH-covered surface, because in that case the proton transfer from an adsorbed OOH species to the surface is blocked, which leads to a higher overpotential. However, the Pourbaix diagram shows that a fully OH-covered surface is unlikely to be present under typical OER conditions.

SUMMARY

Although rutile RuO₂ is usually assumed to be non-magnetic (NM), it is in fact an anti-ferromagnetic (AFM) metal at room temperature according to the recent literature. By means of density functional theory (DFT) calculations, applying the DFT+U formalism, we model the oxygen evolution reaction (OER) on the AFM RuO₂(110) surface and contrast our results with those obtained for NM RuO₂. Although magnetic ordering as such is not expected to play a role in chemical bonding, the presence of magnetic moments on the Ru atoms changes their electronic structure considerably, as compared with the low-spin NM state, which affects their bonding to adsorbed species.

The RuO₂(110) surface is known to be covered by O or OH groups, or a mixture of the two, depending on the pH and on

the applied potential. We model the thermodynamic stability of these possible coverages and the effect they have on the free energies of the OER steps. We find that different coverages have little effect on the overpotential calculated for the OER on an AFM RuO₂(110), with values between 0.41 and 0.49 V. The adsorption energies of the intermediate species involved in the OER (OH, O, and OOH) on the active Ru sites on the surface vary little with different O/OH coverages. This indicates that it is the local electronic structure of the active Ru site which determines the reaction energies and that this electronic structure does not change very much upon altering the surface coverage.

The exception is a 100% OH-covered surface, which gives a significantly higher overpotential of 0.71 V. This is due to blocking the proton transfer from the adsorbed OOH species to the surface in this particular case. However, such a coverage is not stable at the potentials required to drive the OER, where (part of) the surface is converted to O-coverage, which allows for the proton transfer, and lowers the overpotential.

In contrast, a NM RuO₂(110) surface gives significantly higher overpotentials of 0.63–0.67 V for mixed O/OH terminations. It demonstrates that representing the magnetic moments on the Ru atoms is necessary to describe their electronic structure properly and capture accurately the bonding to the intermediate species involved in the OER. The overpotential calculated for AFM RuO₂(110) is not only low but also remarkably insensitive to different surface terminations, which adds to the reasons why RuO₂ is an excellent OER catalyst.

■ ASSOCIATED CONTENT

Supporting Information

The Supporting Information is available free of charge at <https://pubs.acs.org/doi/10.1021/acs.jpcc.1c08700>.

Figures S1–S3 and Tables S1–S3 describe the structure and magnetic structure of the RuO₂ bulk and (110) surface and the results of convergence tests regarding the size of the slab and supercell used to represent this surface. Figure S4 visualizes the OER reaction cycle on a fully OH-terminated RuO₂(110) surface. Figures S5 and S6 show the results of calculations using a smaller, 2 × 1 surface supercell. Figure S7 shows the adsorption energies of the intermediate species as calculated for NM RuO₂ (PDF)

■ AUTHOR INFORMATION

Corresponding Authors

Anja Bieberle-Hütter – *Electrochemical Materials and Interfaces (EMI), Dutch Institute for Fundamental Energy Research (DIFFER), 5612 AJ, Eindhoven, The Netherlands; Center for Computational Energy Research (CCER), 5600 MB, Eindhoven, The Netherlands; orcid.org/0000-0001-8794-9312; Email: a.bieberle@diff.nl*

Geert Brocks – *Center for Computational Energy Research (CCER), 5600 MB, Eindhoven, The Netherlands; Materials Simulation and Modeling (MSM), Department of Applied Physics, Eindhoven University Technology, 5600 MB, Eindhoven, The Netherlands; Computational Materials Science, Faculty of Science and Technology and MESA+ Institute for Nanotechnology, University of Twente, 7500 AE, Enschede, The Netherlands; Email: g.h.l.a.brocks@utwente.nl*

Author

Qjuhua Liang – *Electrochemical Materials and Interfaces (EMI), Dutch Institute for Fundamental Energy Research (DIFFER), 5612 AJ, Eindhoven, The Netherlands; Materials Simulation and Modeling (MSM), Department of Applied Physics, Eindhoven University Technology, 5600 MB, Eindhoven, The Netherlands; orcid.org/0000-0002-5436-5203*

Complete contact information is available at: <https://pubs.acs.org/10.1021/acs.jpcc.1c08700>

Notes

The authors declare no competing financial interest.

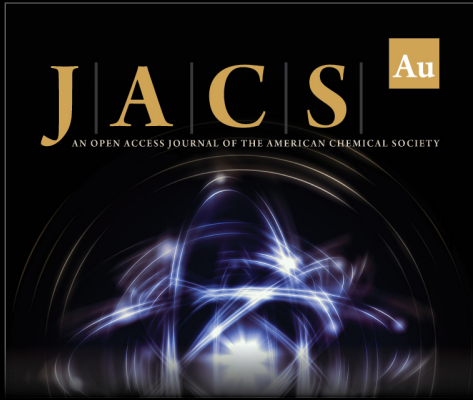
■ ACKNOWLEDGMENTS

Q.L. acknowledges funding from the China Scholarship Council (CSC) (No. 201708450082). A.B.-H. acknowledges the financial support from M-ERA.NET (project “MuMo4-PEC” no. 4089). This work was carried out on the Dutch national e-infrastructure with the support of SURF Cooperative. Michael Verhage and Dr. Kees Flipse, Technical University Eindhoven, The Netherlands, as well as Dr. Gilles de Wijs, Radboud University, are thanked for fruitful discussions. A preliminary version of the present work can be found in Q.L.’s thesis.²⁰

■ REFERENCES


- (1) Song, J.; Wei, C.; Huang, Z.-F.; Liu, C.; Zeng, L.; Wang, X.; Xu, Z. J. A review on fundamentals for designing oxygen evolution electrocatalysts. *Chem. Soc. Rev.* **2020**, *49*, 2196–2214.
- (2) Suen, N.-T.; Hung, S.-F.; Quan, Q.; Zhang, N.; Xu, Y.-J.; Chen, H. M. Electrocatalysis for the oxygen evolution reaction: recent development and future perspectives. *Chem. Soc. Rev.* **2017**, *46*, 337–365.
- (3) Zhang, X.; Bieberle-Hütter, A. Modeling and Simulations in Photoelectrochemical Water Oxidation: From Single Level to Multiscale Modeling. *ChemSusChem* **2016**, *9*, 1223–1242.
- (4) Roy, C.; Rao, R. R.; Stoerzinger, K. A.; Hwang, J.; Rossmeisl, J.; Chorkendorff, I.; Shao-Horn, Y.; Stephens, I. E. L. Trends in Activity and Dissolution on RuO₂ under Oxygen Evolution Conditions: Particles versus Well-Defined Extended Surfaces. *ACS Energy Lett.* **2018**, *3*, 2045–2051.
- (5) Rao, R. R.; Kolb, M. J.; Halck, N. B.; Pedersen, A. F.; Mehta, A.; You, H.; Stoerzinger, K. A. Towards identifying the active sites on RuO₂(110) in catalyzing oxygen evolution. *Energy Environ. Sci.* **2017**, *10*, 2626–2637.
- (6) Rao, R. R.; Kolb, M. J.; Giordano, L.; Pedersen, A. F.; Katayama, Y.; Hwang, J.; Mehta, A. Operando identification of site-dependent water oxidation activity on ruthenium dioxide single-crystal surfaces. *Nat. Catal.* **2020**, *3*, 516–525.
- (7) Ge, R.; Li, L.; Su, J.; Lin, Y.; Tian, Z.; Chen, L. Ultrafine Defective RuO₂ Electrocatalyst Integrated on Carbon Cloth for Robust Water Oxidation in Acidic Media. *Adv. Energy Mater.* **2019**, *9*, 1901313.
- (8) Ryden, W. D.; Lawson, A. W. Magnetic Susceptibility of IrO₂ and RuO₂. *J. Chem. Phys.* **1970**, *52*, 6058–6061.
- (9) Riga, J.; Tenret-Noel, C.; Pireaux, J.-J.; Caudano, R.; Verbist, J.; Gobillon, Y. Electronic structure of rutile oxides TiO₂, RuO₂ and IrO₂ studied by X-ray photoelectron spectroscopy. *Phys. Scr.* **1977**, *16*, 351.
- (10) Zagalskaya, A.; Alexandrov, V. Role of Defects in the Interplay between Adsorbate Evolving and Lattice Oxygen Mechanisms of the Oxygen Evolution Reaction in RuO₂ and IrO₂. *ACS Catal.* **2020**, *10*, 3650–3657.
- (11) Klyukin, K.; Zagalskaya, A.; Alexandrov, V. Role of Dissolution Intermediates in Promoting Oxygen Evolution Reaction at RuO₂(110) Surface. *J. Phys. Chem. C* **2019**, *123*, 22151–22157.


- (12) Rossmeisl, J.; Qu, Z. W.; Zhu, H.; Kroes, G. J.; Nørskov, J. K. Electrolysis of water on oxide surfaces. *J. Electroanal. Chem.* **2007**, *607*, 83–89.
- (13) Fang, Y.-H.; Liu, Z.-P. Mechanism and Tafel Lines of Electro-Oxidation of Water to Oxygen on RuO₂(110). *J. Am. Chem. Soc.* **2010**, *132*, 18214–18222.
- (14) Berlijn, T.; Snijders, P. C.; Delaire, O.; Zhou, H. D.; Maier, T. A.; Cao, H. B.; Chi, S. X. Itinerant Antiferromagnetism in RuO₂. *Phys. Rev. Lett.* **2017**, *118*, No. 077201.
- (15) Torun, E.; Fang, C. M.; de Wijs, G. A.; de Groot, R. A. Role of Magnetism in Catalysis: RuO₂ (110) Surface. *J. Phys. Chem. C* **2013**, *117*, 6353–6357.
- (16) Over, H.; Kim, Y. D.; Seitsonen, A. P.; Wendt, S.; Lundgren, E.; Schmid, M.; Varga, P.; Morgante, A.; Ertl, G. Atomic-Scale Structure and Catalytic Reactivity of the RuO₂ (110) Surface. *Science* **2000**, *287*, 1474–1476.
- (17) Mu, R.; Cantu, D. C.; Lin, X.; Glezakou, V.-A.; Wang, Z.; Lyubinetzky, I.; Rousseau, R.; Dohnálek, Z. Dimerization Induced Deprotonation of Water on RuO₂(110). *J. Phys. Chem. Lett.* **2014**, *5*, 3445–3450.
- (18) Mu, R.; Cantu, D. C.; Glezakou, V.-A.; Lyubinetzky, I.; Rousseau, R.; Dohnálek, Z. Deprotonated Water Dimers: The Building Blocks of Segmented Water Chains on Rutile RuO₂(110). *J. Phys. Chem. C* **2015**, *119*, 23552–23558.
- (19) Kuo, D.-Y.; Paik, H.; Kloppenburg, J.; Faeth, B.; Shen, K. M.; Schlom, D. G.; Hautier, G.; Suntivich, J. Measurements of Oxygen Electrodesorption Energies and Oxygen Evolution Reaction on RuO₂(110): A Discussion of the Sabatier Principle and Its Role in Electrocatalysis. *J. Am. Chem. Soc.* **2018**, *140*, 17597–17605.
- (20) Liang, Q. *First-Principles Study of Electrode Materials for Oxygen Evolution*; Eindhoven University of Technology: Eindhoven, The Netherlands, 2021.
- (21) Blöchl, P. E. Projector augmented-wave method. *Phys. Rev. B* **1994**, *50*, 17953–17979.
- (22) Kresse, G.; Joubert, D. From ultrasoft pseudopotentials to the projector augmented-wave method. *Phys. Rev. B* **1999**, *59*, 1758–1775.
- (23) Kresse, G.; Furthmüller, J. Efficient iterative schemes for ab initio total-energy calculations using a plane-wave basis set. *Phys. Rev. B* **1996**, *54*, 11169–11186.
- (24) Perdew, J. P.; Burke, K.; Ernzerhof, M. Generalized Gradient Approximation Made Simple. *Phys. Rev. Lett.* **1996**, *77*, 3865–3868.
- (25) Dudarev, S. L.; Botton, G. A.; Savrasov, S. Y.; Humphreys, C. J.; Sutton, A. P. Electron-energy-loss spectra and the structural stability of nickel oxide: An LSDA+U study. *Phys. Rev. B* **1998**, *57*, 1505–1509.
- (26) Mattheiss, L. F. Electronic structure of RuO₂, OsO₂, and IrO₂. *Phys. Rev. B* **1976**, *13*, 2433–2450.
- (27) Monkhorst, H. J.; Pack, J. D. Special points for Brillouin-zone integrations. *Phys. Rev. B* **1976**, *13*, 5188–5192.
- (28) Kim, Y. D.; Seitsonen, A. P.; Over, H. The atomic geometry of oxygen-rich Ru(0001) surfaces: coexistence of (1 × 1)O and RuO₂(110) domains. *Surf. Sci.* **2000**, *465*, 1–8.
- (29) Nørskov, J. K.; Rossmeisl, J.; Logadottir, A.; Lindqvist, L.; Kitchin, J. R.; Bligaard, T.; Jónsson, H. Origin of the Overpotential for Oxygen Reduction at a Fuel-Cell Cathode. *J. Phys. Chem. B* **2004**, *108*, 17886–17892.
- (30) Asthagiri, A.; Janik, M. J. *Computational catalysis*; Royal Society of Chemistry: 2013.
- (31) van Setten, M. J.; de Wijs, G. A.; Brocks, G. First-principles calculations of the crystal structure, electronic structure, and thermodynamic stability of Be(BH₄)₂. *Phys. Rev. B* **2008**, *77*, 165115.
- (32) Liang, Q.; Brocks, G.; Bieberle-Hütter, A. Oxygen evolution reaction (OER) mechanism under alkaline and acidic conditions. *J. Phys. Energy* **2021**, *3*, No. 026001.
- (33) Rong, X.; Parolin, J.; Kolpak, A. M. A Fundamental Relationship between Reaction Mechanism and Stability in Metal Oxide Catalysts for Oxygen Evolution. *ACS Catal.* **2016**, *6*, 1153–1158.
- (34) Song, F.; Bai, L.; Moysiadou, A.; Lee, S.; Hu, C.; Liardet, L.; Hu, X. Transition Metal Oxides as Electrocatalysts for the Oxygen Evolution Reaction in Alkaline Solutions: An Application-Inspired Renaissance. *J. Am. Chem. Soc.* **2018**, *140*, 7748–7759.
- (35) Briquet, L. G. V.; Sarwar, M.; Mugo, J.; Jones, G.; Calle-Vallejo, F. A New Type of Scaling Relations to Assess the Accuracy of Computational Predictions of Catalytic Activities Applied to the Oxygen Evolution Reaction. *ChemCatChem* **2017**, *9*, 1261–1268.
- (36) Liang, Q.; Brocks, G.; Zhang, X.; Bieberle-Hütter, A. Monolayer Nitrides Doped with Transition Metals as Efficient Catalysts for Water Oxidation: The Singular Role of Nickel. *J. Phys. Chem. C* **2019**, *123*, 26289–26298.
- (37) Fidelsky, V.; Toroker, M. C. Enhanced Water Oxidation Catalysis of Nickel Oxyhydroxide through the Addition of Vacancies. *J. Phys. Chem. C* **2016**, *120*, 25405–25410.
- (38) Kishore, R.; Cao, X.; Zhang, X.; Bieberle-Hütter, A. Electrochemical water oxidation on WO₃ surfaces: A density functional theory study. *Catal. Today* **2019**, *321–322*, 94–99.
- (39) Diaz-Morales, O.; Ledezma-Yanez, I.; Koper, M. T. M.; Calle-Vallejo, F. Guidelines for the Rational Design of Ni-Based Double Hydroxide Electrocatalysts for the Oxygen Evolution Reaction. *ACS Catal.* **2015**, *5*, 5380–5387.
- (40) Zhang, P.; Dong, Y.; Kou, Y.; Yang, Z.; Li, Y.; Sun, X. First-Principles Study of Oxygen Evolution Reaction on the Oxygen-Containing Species Covered CoII-Exposing Co₃O₄ (100) Surface. *Catal. Lett.* **2015**, *145*, 1169–1176.



JACS Au
AN OPEN ACCESS JOURNAL OF THE AMERICAN CHEMICAL SOCIETY

Editor-in-Chief
Prof. Christopher W. Jones
Georgia Institute of Technology, USA

Open for Submissions 

pubs.acs.org/jacsau  ACS Publications
Most Trusted. Most Cited. Most Read.